

ACCELERATING LANGEVIN SAMPLING WITH BIRTH-DEATH

YULONG LU, JIANFENG LU, AND JAMES NOLEN

ABSTRACT. A fundamental problem in Bayesian inference and statistical machine learning is to efficiently sample from multimodal distributions. Due to metastability, multimodal distributions are difficult to sample using standard Markov chain Monte Carlo methods. We propose a new sampling algorithm based on a birth-death mechanism to accelerate the mixing of Langevin diffusion. Our algorithm is motivated by its mean field partial differential equation (PDE), which is a Fokker-Planck equation supplemented by a nonlocal birth-death term. This PDE can be viewed as a gradient flow of the Kullback-Leibler divergence with respect to the Wasserstein-Fisher-Rao metric. We prove that under some assumptions the asymptotic convergence rate of the nonlocal PDE is independent of the potential barrier, in contrast to the exponential dependence in the case of the Langevin diffusion. We illustrate the efficiency of the birth-death accelerated Langevin method through several analytical examples and numerical experiments.

1. INTRODUCTION

Numerical sampling of high dimensional probability distributions with unknown normalization has important applications in machine learning, Bayesian statistics, computational physics, and other related fields. The most popular approaches are based on Markov chain Monte Carlo (MCMC), including Langevin MCMC [40], underdamped Langevin MCMC [20], Hamiltonian Monte Carlo [41, 1, 36], bouncy particle and zigzag samplers [4, 3], etc. Many of these approaches, often combined with stochastic gradient [45, 30], have been widely used in machine learning.

When the target probability distribution is (strongly) log-concave, that is, when its density with respect to the Lebesgue measure is $\pi(x) \propto e^{-V(x)}$ with V being (strongly) convex, it is known that most sampling schemes mentioned above can produce independent random samples efficiently [12, 15, 31, 9, 16]. The sampling problem becomes much more challenging when the probability distribution exhibits multi-modality, as it takes much longer time for the sampling Markov chain to get through low-probability regions in the phase space to explore and balance between multiple modes (also known as metastability). Many enhanced sampling schemes have been proposed over the years to overcome such difficulty, including various tempering schemes [43, 19, 32, 35], biasing techniques [44, 24], non-equilibrium sampling [37], just to name a few.

In this work, we propose a simple, novel sampling dynamics to overcome the metastability based on birth-death process. On the continuous level of evolution of the probability density, the proposed dynamics is given by

$$(1) \quad \partial_t \rho_t = \underbrace{\nabla \cdot (\nabla \rho_t + \rho_t \nabla V)}_{\text{overdamped Langevin}} + \underbrace{\rho_t (\log \pi - \log \rho_t) - \rho_t \mathbb{E}_{\rho_t} (\log \pi - \log \rho_t)}_{\text{birth-death}},$$

where one adds a non-local (due to the expectation) update rule to the conventional overdamped Langevin dynamics. The advantage of the birth-death process is that it allows global move of the mass of a probability density directly from one mode to another in the phase space according to their relative weights, without the difficulty of going through low probability regions, suffered by any local dynamics such as the overdamped Langevin MCMC. It is possible to combine the birth-death process with other sampling dynamics, such as underdamped Langevin or various accelerated dynamics, while for simplicity of presentation we will focus only on the birth-death accelerated overdamped Langevin dynamics in the current work.

1.1. Contribution. Our main theoretical result is that under mild assumptions the asymptotic convergence rate of the proposed sampling dynamics is independent of the barrier of the potential corresponding to the target measure – this is a substantial improvement of the convergence rate of

overdamped Langevin diffusion, which is exponentially small due to metastability. Moreover, we also establish a gradient flow structure of the birth-death accelerated Langevin dynamics: it is a gradient flow of the Kullback-Leibler (KL)-divergence with respect to the Wasserstein-Fisher-Rao metric.

To demonstrate this improved convergence, we study two analytical examples showing significant speedup of mixing compared to Langevin diffusion. We also propose a practical interacting particle sampling scheme as a numerical implementation of the birth-death accelerated Langevin dynamics. The efficiency of the proposed algorithm is illustrated through several numerical examples.

1.2. Related works. The proposed sampling scheme involves interacting particles that undergo Langevin diffusion and birth-death process. Other sampling schemes via interacting particles have been proposed recently, including the Stein variational gradient descent (SVGD) flow [28, 27] (see also its continuous limit studied in [29]). Unlike the samplers based on Stein discrepancy, which replaces the random noise in Langevin dynamics by repulsion of particles, the sampling scheme proposed in this work employs birth-death process to enhance the mixing of existing sampling schemes. In fact, it can also be potentially combined with SVGD to improve its convergence.

The birth-death process has been used in sequential Monte Carlo (SMC) samplers [14]. In SMC, the birth-death and branching process is used to reduce the variance of particle weights. While in the current proposed scheme, it is used to globally move the sampling particles according to the target measure. The birth-death process is also used recently to accelerate training of neural networks in the mean-field regime [42], also for a quite different purpose than accelerating convergence of Monte Carlo samplers.

Acknowledgement. The work of Jianfeng Lu and the work of James Nolen were partially funded through grants DMS-1454939 and DMS-1351653 from the National Science Foundation, respectively.

2. FOKKER-PLANCK EQUATION AND BIRTH-DEATH PROCESS

2.1. Langevin dynamics and its Fokker-Planck equation. Recall the (overdamped) Langevin diffusion is the solution to the following stochastic differential equation

$$(2) \quad dX_t = -\nabla V(X_t)dt + \sqrt{2}dW_t,$$

where $X_t \in \mathbb{R}^d$ and W_t is a d -dimensional Brownian motion. Many popular sampling schemes are constructed from discretizations of (2), such as the unadjusted Langevin algorithm (ULA) and its Metropolized version – Metropolis-adjusted Langevin algorithm (MALA) [40]. The probability density function $\rho_t(x)$ of (2) solves the linear Fokker-Planck equation (FPE) on \mathbb{R}^d

$$(3) \quad \partial_t \rho_t = \nabla \cdot (\nabla \rho_t + \rho_t \nabla V).$$

The stationary distribution of (2) and (3) has density $\pi(x) = e^{-V(x)}/Z$. In the seminal work of Jordan-Kinderlehrer-Otto [22], the FPE (3) was identified as the gradient flow of the KL-divergence (*i.e.*, relative entropy) $\text{KL}(\rho|\pi) = \int \rho \log(\rho/\pi) dx$, with respect to the 2-Wasserstein distance. Moreover, if the target measure π satisfies the logarithmic Sobolev inequality (LSI): for any probability distribution ρ ,

$$(4) \quad \text{KL}(\rho|\pi) \leq \frac{1}{\lambda} \mathcal{I}(\rho|\pi) \text{ with the relative Fisher information } \mathcal{I}(\rho|\pi) = \int \rho |\nabla \log(\rho/\pi)|^2 dx,$$

then we have the exponential convergence $\text{KL}(\rho_t|\pi) \leq e^{-\lambda t} \text{KL}(\rho_0|\pi)$. The convergence rate λ above may be exponentially small though when the target distribution is multimodal with high potential barrier; see [5, 6].

2.2. Pure birth-death process. The main idea of this work is to use birth-death process to accelerate sampling. Before combining it with the Langevin dynamics, let us consider the pure birth-death equation (BDE) given by

$$(5) \quad \partial_t \rho_t = -\alpha_t \rho_t, \quad \text{with} \quad \alpha_t(x) := \log \rho_t(x) - \log \pi(x) - \int_{\mathbb{R}^d} (\log \rho_t - \log \pi) \rho_t dy.$$

As there is no spatial derivative involved in (5), it can be viewed as a (infinite) system of ordinary differential equations, indexed by $x \in \mathbb{R}^d$, coupled through the integral term in α_t . Observe that π is an invariant measure of (5). Moreover, equation (5) depends on π only up to a multiplicative constant, making it feasible for sampling π with an unknown normalization constant. The definition of the birth/death rate $\alpha_t(x)$ in (5) is very intuitive. In fact, ignoring the last integral term in the definition of α_t , one sees that the solution ρ_t to (5) adjusts the mass according to the difference of the logarithm of current density and that of the target: the density $\rho_t(x)$ at a location x increases (or decreases) if $\rho_t(x) < \pi(x)$ (or $\rho_t(x) > \pi(x)$). The integral term in (5) is added to guarantee that the total integral of ρ_t is conserved during the evolution, and thus ρ_t remains a probability distribution (positivity is also to verify).

The birth-death dynamics (5) differs substantially from FPE (3) in many aspects. The former is essentially a nonlinear system of ODEs (but with a non-local coefficient) whereas the later is a linear parabolic PDE. Due to the absence of diffusion, the support of the solution ρ_t of (5) never increases during the evolution. This seems suggesting that the birth-death equation is unsuitable for sampling. However, we shall show in Theorem 3.4 that if the initial density is positive everywhere, then ρ_t converges to π as $t \rightarrow \infty$.

2.3. Fokker-Planck equation with birth-death dynamics. The real power of the birth-death process above comes in when it is combined with the Fokker-Planck equation (3), which yields the following equation on the level of probability density, already appeared in the introduction:

$$(6) \quad \partial_t \rho_t = \nabla \cdot (\nabla \rho_t + \rho_t \nabla V) - \alpha_t \rho_t,$$

where $\alpha_t = \log \rho_t - \log \pi - \int_{\mathbb{R}^d} (\log \rho_t - \log \pi) \rho_t dx$. Before we discuss the discretization of (6) in Section 5, which will lead to an efficient particle sampler in practice, in what follows, we study the Fokker-Planck equation of birth-death accelerated Langevin dynamics (BDL-FPE) (6), in particular its favorable convergence properties compared to the original Langevin dynamics (3) and the pure birth-death process (5).

3. ANALYSIS OF THE FOKKER-PLANCK EQUATION WITH BIRTH-DEATH

3.1. Gradient flow structure. In parallel to well-known fact that FPE (3) is the 2-Wasserstein gradient flow of the KL-divergence, BDL-FPE (6) can be viewed as a gradient flow of the KL-divergence with respect to a different metric. Our result is motivated by recent works on the Wasserstein-Fisher-Rao (WFR) distance [23, 10, 26, 33] in the study of unbalanced optimal transport. Specifically, we define the Wasserstein-Fisher-Rao distance (also known as the spherical Hellinger-Kantorovich distance [23, 7]) by

$$(7) \quad d_{\text{WFR}}^2(\rho_0, \rho_1) = \inf_{\rho_t, u_t \in \mathcal{A}_{\text{WFR}}(\rho_0, \rho_1)} \int_0^1 \left(\int |\nabla u_t|^2 + |u_t|^2 d\rho_t - \left(\int u_t \rho_t dx \right)^2 \right) dt,$$

where the admissible set $\mathcal{A}_{\text{WFR}}(\rho_0, \rho_1)$ consists of all pairs $(\rho_t, u_t) \in \mathcal{P}(\mathbb{R}^d) \times L^2(\mathbb{R}^d, d\rho_t)$ such that $\{\rho_t\}_{t \in [0,1]}$ is a narrowly continuous curve in $\mathcal{P}(\mathbb{R}^d)$ connecting ρ_0 and ρ_1 and that

$$(8) \quad \partial_t \rho_t = \nabla \cdot (\rho_t \nabla u_t) - \rho_t (u_t - \int_{\mathbb{R}^d} u_t \rho_t dx) \text{ in the weak sense.}$$

Here $\mathcal{P}(\mathbb{R}^d)$ denotes the space of probability measures on \mathbb{R}^d and $L^2(\mathbb{R}^d, d\rho_t)$ is the space of functions u satisfying $\int u^2(x) \rho_t(x) dx < \infty$. We emphasize that for our sampling purpose we have modified the original definition of WFR distance in [2, 23, 10] by adding the integral penalty term to keep mass conserved. Without this term, ρ_t may experience gain and loss of mass during transportation procedure. Our first result is the following theorem which characterizes the gradient flow structure of BDL-FPE (6), whose proof is provided in Appendix A.

Theorem 3.1. *The Fokker-Planck equation for birth-death accelerated Langevin (BDL-FPE) dynamics (6) is the gradient flow of the KL-divergence $\text{KL}(\cdot|\pi)$ with respect to the Wasserstein-Fisher-Rao distance (7).*

As a consequence of Theorem 3.1, the dynamics (6) dissipates the KL-divergence in a steepest descent manner with respect to the WFR metric (7), similar to the variational structure for the Fokker-Planck equation (3) (w.r.t. the 2-Wasserstein metric).

3.2. Convergence analysis. We now analyze the convergence of BDL-FPE (6). Proofs of results in this section can be found in Appendix B. We first establish in the following theorem the global convergence of (6) by assuming the validity of LSI (4).

Theorem 3.2. *Assume that π satisfies the log-Sobolev inequality (4) with constant $\lambda > 0$. Then the solution ρ_t to BDL-FPE (6) with initial condition ρ_0 satisfies*

$$(9) \quad \text{KL}(\rho_t|\pi) \leq e^{-\lambda t} \text{KL}(\rho_0|\pi).$$

Theorem 3.2 shows that the global convergence rate of BDL-FPE (6) can be no worse than that of FPE (3). The convergence rate obtained this way is fully characterized by the log-Sobolev constant though, which may scale badly when the potential V has high potential barriers. In contrast, we show in the next theorem that the birth-death term accelerates the diffusion dramatically in the sense that the asymptotic convergence rate of BDL-FPE (6) is independent of the potential barrier of V .

Theorem 3.3. *Let ρ_t solve (6) for $t \geq t_0$, with initial condition satisfying $\text{KL}(\rho_{t_0}|\pi) \leq 1$. Suppose that for some $M \geq 1$,*

$$(10) \quad \inf_{x \in \mathbb{R}^d} \frac{\rho_{t_0}(x)}{\pi(x)} \geq e^{-M}$$

also holds. Then, for any $\delta \in (0, 1/4)$,

$$(11) \quad \text{KL}(\rho_t|\pi) \leq e^{-(2-3\delta)(t-t_*)} \text{KL}(\rho_{t_0}|\pi)$$

holds for all $t \geq t_* = t_0 + \log(\frac{M}{\delta^3})$. In particular, the BDL-FPE (6) has an asymptotic convergence rate which is independent of the potential V corresponding to π .

Theorem 3.3 states that as long as the solution ρ_t of BDL-FPE (6) is not too far from the target ($\text{KL}(\rho_t|\pi) \leq 1$) and satisfies a uniform lower bound (maybe tiny) with respect to π starting from t_0 , it will converge to π with a rate independent of V after a short waiting time. In practice, t_0 can be chosen $O(1)$ to satisfy the condition (10); see Section 4 for examples.

For completeness, we also show the global convergence of BDE (5) (without a rate) in the next theorem. The BDE also has a similar gradient flow structure; we will not go into details here.

Theorem 3.4. *Let ρ_t be the solution to (5) with initial condition ρ_0 . Assume that $\log \pi(x)$ is finite for any $x \in \mathbb{R}^d$. Assume also that ρ_0 satisfies that $\text{KL}(\rho_0|\pi) < \infty$ and $\rho_0(x) > 0$ for all $x \in \mathbb{R}^d$. Then $\rho_t(x) > 0$ for all $x \in \mathbb{R}^d$ and $t > 0$. Moreover, for all $x \in \mathbb{R}^d$, $\lim_{t \rightarrow \infty} \rho_t(x) = \pi(x)$ and $\lim_{t \rightarrow \infty} \text{KL}(\rho_t|\pi) = 0$.*

4. ILLUSTRATIVE EXAMPLES

Here we present two very simple examples illustrating how the combined dynamics of BDL-FPE (6) may significantly enhance convergence to equilibrium, compared to either FPE (3) or BDE (5).

4.1. Uniform distribution on torus. Let $L \gg 1$, and suppose the domain is the d -dimensional torus $\mathbb{T}_L^d = [0, L]^d$ with $\pi(x) \equiv L^{-d}$ being the density of the uniform measure on \mathbb{T}_L^d . In this case, FPE dynamics (3) corresponds to the heat equation $\partial_t w = \Delta w$ on \mathbb{T}_L^d . The spectral gap is $O(L^{-2})$, and hence the rate of convergence to the equilibrium measure is $O(L^{-2})$. While this convergence rate is slow for large L , the FPE dynamics (3) may be used to prepare a good initial condition for the combined BDL-FPE dynamics (6). Specifically, a lower bound on the heat kernel shows that at time $t = 1$ the solution to $\partial_t w = \Delta w$ will satisfy

$$\inf_{x \in \mathbb{T}_L^d} w(1, x) \geq (c_1)^{d/2} e^{-dL^2}.$$

for a universal constant $c_1 > 0$, that is independent of the initial data (assuming it is a probability measure) and the dimension d . Then, if we use $\rho_1(x) = w(1, x)$ as initial data for the combined

dynamics (6), for $t \geq t_0 = 1$, the condition (10) holds with $M = O(dL^2)$. If $\text{KL}(\rho_{t_0}|\pi) \leq 1$ also holds, Theorem (3.3) then implies $\text{KL}(\rho_t|\pi) \leq e^{-(t-t_*)}$ for $t \geq t_* = t_0 + O(\log d) + O(\log L)$. In particular, the convergence rate does not depend on L and the time lag $(t_* - t_0)$ is $O(\log L)$ rather than $O(L^2)$.

4.2. Double well. Suppose $\pi(x) = Z^{-1}e^{-V(x)}$ with $V(x) = \epsilon^{-1} \cos^2(\pi x)$, $x \in [-1, 1]$, for some $\epsilon > 0$. Here we regard $\pi(x)$ as a density on the one-dimensional torus $\mathbb{T}^1 = [-1, 1]$. This density has two modes at $x = \pm 1/2$. Moreover, $\max V - \min V = \epsilon^{-1}$. It is known that for this potential V , the FPE dynamics (3) exhibits a metastability phenomenon, and the mixing time for pure Langevin dynamics is $O(e^{C\epsilon^{-1}})$ for $\epsilon \ll 1$ (see [5, 6, 34]).

Suppose that the initial density ρ_0 is the restriction of $\pi(x)$ to the region $[-1, 0]$:

$$(12) \quad \rho_0(x) = 2\pi(x)\mathbb{1}_{[-1,0]}.$$

Then $\text{KL}(\rho_0|\pi) = \log 2 < 1$. If ρ_t evolves according to pure Langevin dynamics (3) for $t \in [0, 1]$, a lower bound on the heat kernel (via a large deviation type estimate [17], or by [38]) implies that at $t = 1$,

$$\inf_{x \in [-1, 1]} \rho_1(x) \geq C_1 e^{-C_2 \epsilon^{-2}}$$

for some positive constants C_1 and C_2 . Then, suppose that for $t \geq t_0 = 1$, ρ_t evolves according to the combined dynamics (6). Theorem (3.3) implies that for $t \geq t_* = 1 + O(|\log \epsilon|)$, we have $\text{KL}(\rho_t|\pi) \leq e^{-(t-t_*)}$. So, compared to the solution to the Langevin dynamics (3), the birth-death accelerated dynamics (6) exhibits a dramatic acceleration and converges to $\pi(x)$ at a rate that is independent of ϵ after a brief delay of $O(\log \epsilon)$.

5. AN INTERACTING PARTICLE IMPLEMENTATION

As we mentioned earlier, the FPE (3) has a nice particle interpretation since it is the probability density function of the Langevin diffusion (2). The dynamics of BDL-FPE (6) does not have such a simple particle interpretation, due to the logarithmic nonlinearity in the birth-death term. To resolve this difficulty, given a smooth kernel function $K(x)$ approximating the Dirac delta, we might approximate (6) by the equation

$$(13) \quad \begin{aligned} \partial_t \rho_t &= \nabla \cdot (\nabla \rho_t + \rho_t \nabla V) - \Lambda(x, \rho_t) \rho_t, \\ \text{where } \Lambda(x, \rho_t) &= \log(K * \rho_t) - \log \pi - \int_{\mathbb{R}^d} \log\left(\frac{(K * \rho_t)}{\pi}\right) \rho_t dx. \end{aligned}$$

For this equation, the solution ρ_t can be approximated by the empirical measure μ_t^N of a collection of interacting particles $\{x_t^i\}_{i=1}^N$ evolving as follows ($\mu_t^N = \frac{1}{N} \sum_{i=1}^N \delta_{x_t^i}$):

Step 1: between birth/death events, each particle x^i diffuses independently according to (2).

Step 2: each particle also has an independent exponential clock with instantaneous birth-death rate

$$(14) \quad \begin{aligned} \Lambda(x_t^i) &= \log\left(\frac{1}{N} \sum_{j=1}^N K(x_t^i - x_t^j)\right) - \log \pi(x_t^i) - \frac{1}{N} \sum_{\ell=1}^N \left(\log\left(\frac{1}{N} \sum_{j=1}^N K(x_t^\ell - x_t^j)\right) - \log \pi(x_t^\ell)\right) \\ &= \log((K * \mu_t^N)(x_t^i)) - \log \pi(x_t^i) - \int_{\mathbb{R}^d} \log\left(\frac{K * \mu_t^N}{\pi}\right) d\mu_t^N. \end{aligned}$$

Specifically, if $\Lambda(x_t^i) > 0$, then partial x^i is killed with instantaneous rate $\Lambda(x_t^i)$ and another particle is duplicated randomly to preserve the population size; if $\Lambda(x_t^i) < 0$, then partial x^i is duplicated with instantaneous rate $|\Lambda(x_t^i)|$ and another particle is killed randomly to preserve the population size. Thus the total number of particles is preserved. The proposition below shows convergence of the empirical measure μ_t^N of the particle system described above to the solution of (13) in the large particle limit. Its proof can be found in Appendix B.

Proposition 5.1. *Let μ_t^N be the empirical measure of particles defined above. Assume that $\mu_0^N \rightarrow \rho_0$ as $N \rightarrow \infty$. Then for all $t \in (0, \infty)$, $\mu_t^N \rightarrow \rho_t$ where ρ_t solves (13) with initial condition ρ_0 .*

To implement the birth-death particle dynamics above in practice, we also need time-discretization. In particular, discretizing the Langevin diffusion by the Euler-Maruyama scheme leads to the following birth-death accelerated Langevin sampler (BDLS).

Algorithm 1: BDLS: birth-death accelerated Langevin sampler

Input: A potential $V(x)$ corresponding to the target distribution $\pi(x)$, a set of initial particles $\{x_0^i\}_{i=1}^N$, number of iterations J , time step Δt , kernel function K

Output: A set of particles $\{x_j^i\}_{i=1}^N$ whose empirical measure μ^N approximates π .

```

for  $j = 1 : J$  do
  for  $i = 1 : N$  do
    set  $x_j^i = x_{j-1}^i - \Delta t \nabla V(x_{j-1}^i) + \sqrt{2\Delta t} \xi_j$ , where  $\xi_j \stackrel{\text{i.i.d.}}{\sim} N(0, 1)$ 
    calculate  $\beta_i = \log\left(\frac{1}{N} \sum_{\ell=1}^N K(x_j^i - x_j^\ell)\right) + V(x_j^i)$ 
    set  $\bar{\beta}_i = \beta_i - \frac{1}{N} \sum_{\ell=1}^N \beta_\ell$ 
    if  $\bar{\beta}_i > 0$ 
      kill  $x_j^i$  with probability  $1 - \exp(-\bar{\beta}_i \Delta t)$ ,
      duplicate one particle that is uniformly chosen from the rest
    else if  $\bar{\beta}_i < 0$ 
      duplicate  $x_j^i$  with probability  $1 - \exp(\bar{\beta}_i \Delta t)$ ,
      kill one particle that is uniformly chosen from the rest
    end if
  end for
end for

```

6. NUMERICAL RESULTS

In the numerical examples below, we compare the sampling efficiency of the proposed sampler BDLS of size N with the sampler built from running N independent copies of ULA (we call it parallel ULA or simply ULA for short). We choose the kernel K to be the Gaussian kernel with width h , i.e. $K(x, y) = \frac{1}{(2\pi h^2)^{d/2}} \exp(-|x-y|^2/2h^2)$. The kernel width h varies in different examples and is tuned to produce the best numerical performance. How to optimize the choice of h with a sound theoretical basis is to be investigated in future work.

6.1. Example 1: multimodal distribution on a 1D torus. Consider the target $\pi(x) \propto \exp(-V(x))$ with $V(x) = 2.5 \cos(2x) + 0.5 \sin(x)$ defined on the torus $D := [-2\pi, 2\pi]$. We initialize the continuous dynamics and particle systems according to the Gaussian distribution $\mathcal{N}(0, 0.2)$. This makes sampling the measure π difficult since π has four modes on D , while ρ_0 is very peaked and almost does not overlap with π . We show in the left figure of Figure 1 the convergence of KL-divergence $\text{KL}(\rho_t|\pi)$, from which one sees that BDL-PDE (6) substantially accelerates the slow convergence of FPE (3) of Langevin diffusion, consistent with Theorem 3.3. The reason for fast convergence of BDE (5) is unclear to us and will be investigated in the future. To compare the particle algorithms, we plot in Figure 1 (the middle and right figures) the mean square errors (MSE) of BDLS and ULA in estimating the mean and variance of the target versus number of sample size. We see that BDLS performs much better than ULA. BDS performs the worst in this example (see snapshots in Figure C.5) as due to absence of diffusion the particles only rearrange themselves inside the small region around zero they initialize and never get out. Thus we do not plot the MSE of BDS as they are too large to be fitted in the same figure. We choose the number of particles $N = 100$, time step size $\Delta t = 0.03$ and a Gaussian kernel K with width $h = 0.05$ in this example. See Appendix C for more implementation details and additional numerical results.

6.2. Example 2: two dimensional Gaussian mixture. Consider now a target of two dimensional Gaussian mixture consisting of four components $\pi(x, y) = \sum_{i=1}^4 w_i \mathcal{N}(m_i, \Sigma_i)$ and initial

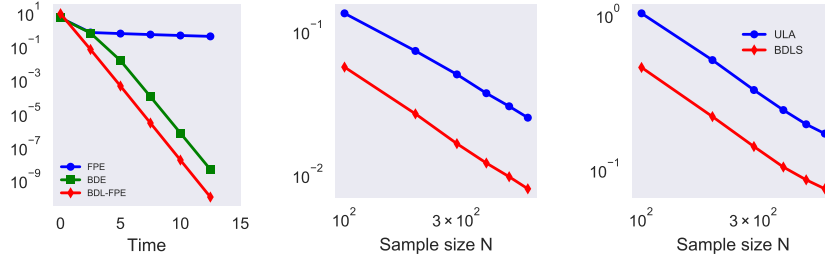


FIGURE 1. Convergence of continuous dynamics and particles systems in Example 1. The left figure shows decay of the KL divergence in semilogy scale along the evolution of three continuous dynamics. The middle (or the right) figure shows the decay in loglog scale of mean square errors of estimating mean (or variance) using varying number of particles.

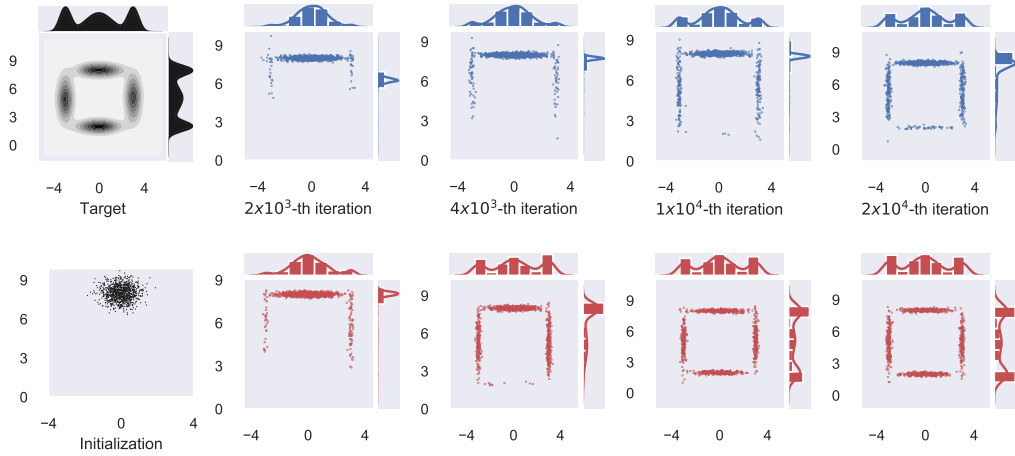


FIGURE 2. Scatter plots of particles and their marginal distributions (computed by kernel density estimators) in Example 2. Top left figure displays the target density and the bottom left shows initial locations of particles. Each column in the rest shows the scatter plots and the marginal distributions of particles computed using parallel ULA (top, blue) and BDLS (bottom, red) at different iterations.

particles sampled from the Gaussian $\mathcal{N}(m_0, \Sigma_0)$, where the parameters are defined by

$$w_i = 1/4, i = 1, \dots, 4, \quad m_0 = m_1 = (0, 8)^T, \quad m_2 = (0, 2)^T, \quad m_3 = (-3, 5)^T, \quad m_4 = (3, 5)^T, \\ \Sigma_1 = \Sigma_2 = \begin{pmatrix} 1.2 & 0 \\ 0 & 0.01 \end{pmatrix}, \quad \Sigma_3 = \Sigma_4 = \begin{pmatrix} 0.01 & 0 \\ 0 & 2 \end{pmatrix}, \quad \Sigma_0 = \begin{pmatrix} 0.3 & 0 \\ 0 & 0.3 \end{pmatrix}.$$

In this example, we choose $N = 10^3$ particles and use time step size $\Delta t = 10^{-3}$ for both ULA and BDLS algorithms. Figure 2 shows scatter plots along with their corresponding marginals of particles computed using parallel ULA and BDLS at different number of iterations. The target distribution has a square shape and the particles are initialized within a small neighborhood of the top edge. At the 10^4 -th iteration, the particles generated by BDLS already start equilibrating around all modes, whereas only very few particles generated by parallel ULA reach to the bottom mode at the same time. We also compare the absolute error of estimating $\mathbb{E}_\pi[f]$ for different f in Figure 3. We find that the estimation errors of using our BDLS converge to the lowest values much faster than ULA.

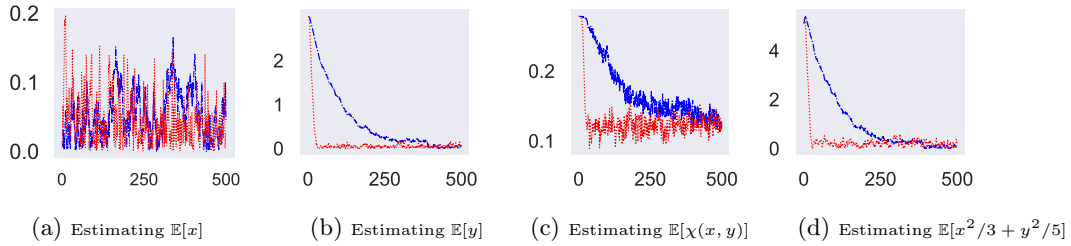


FIGURE 3. The absolute errors of estimating $\mathbb{E}[f(x, y)]$ with various observables f in Example 2. In the third figure $\chi(x, y) = \mathbf{1}_{|x| \leq 5, |y-2| \leq 0.8}$. The blue dash-dot and red-dot lines are estimation errors along iterations using ULA and BDLS respectively. The total number of iterations is 2×10^5 . For the purpose of resolution, we plot the error for every 400 iterations.

6.3. Example 3: Bayesian learning of Gaussian mixture model. We consider the Bayesian approach to fitting the distribution of a dataset with a univariate Gaussian mixture model of three components in the same setting as in [11]. The unknown parameters are the means μ_k , precisions λ_k and the weights $w_k, k = 1, 2, 3$ with $\sum_{k=1}^3 w_k = 1$. We use the prior as in [11] which has a hyperparameter β describing the prior distribution of the precisions, thus defining a posterior distribution π on \mathbb{R}^9 . Due to the permutation invariance with respect to the component label, the resulting posterior has at least $3! = 6$ modes. We generate a synthetic dataset of 200 samples from the mixture measure with “true” parameters $w_1 = w_3 = 1/5, w_2 = 3/5, \mu_1 = -5, \mu_2 = 1, \mu_3 = 6, \lambda_k = 1, k = 1, 2, 3$. The data size is large enough to make the posterior peaked so that hopping across different modes is challenging. We use $N = 2000$ particles, time step size $\Delta t = 1.5 \times 10^{-6}$ and kernel width $h = 1.1$. We initialize particles as iid samples from the following distributions: $(w_1, w_2) \in \text{Dirichlet}_3(1, 1, 1), \mu_k \sim \text{Unif}([3, 7]), \lambda_k \sim \text{Unif}([0.5, 2.5]), \beta \sim \text{Unif}([0.5, 1.5])$. To compare the performance of BDLS and that of ULA, we show the evolution of sampling particles in (μ_1, μ_2) -coordinate in Figure 4 (see also Figure D.8 for snapshots in (w_1, w_2) -coordinate). We see that BDLS algorithm exhibits stronger mode exploration ability than ULA. Once all modes are identified, BDLS quickly redistributes the particles in different local modes towards the equilibrium through the birth-death process, while ULA takes much longer time to equilibrate in the local modes. In fact, the distribution of the BDLS particles in (μ_1, μ_2) at 2×10^4 -th iteration is already very close to the equilibrium (see Figure D.9). Appendix D contains further details about the model and numerical results for this example.

7. CONCLUSION

We propose a new sampling dynamics based on birth-death process and an algorithm based on interacting particles to accelerate the classical Langevin dynamics for statistical sampling. Future directions include a rigorous analysis of the birth-death accelerated Langevin sampler and its further applications when combined with other conventional sampling schemes.

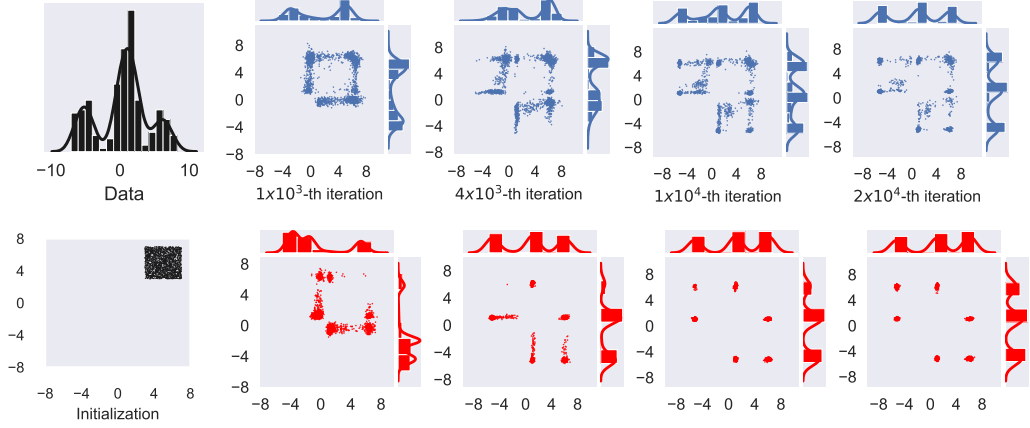


FIGURE 4. Evolution of particles in (μ_1, μ_2) -coordinate for Example 3. The first column shows the histogram (top) of the synthetic data and the initial locations (bottom) of particles in (μ_1, μ_2) -coordinate. The rest columns compare the scatter plots of particles in (μ_1, μ_2) and their marginals computed using parallel ULA (top, blue) and BDLS (bottom, red) at different iterations.

APPENDIX A. GRADIENT FLOW STRUCTURE

This section devotes to the proof of Theorem 3.1. We mainly follow [39] and [18].

We first introduce a Riemannian structure, denoted by \mathcal{M} on the space of smooth probability densities on \mathbb{R}^d . Consider the tangent space at $\rho \in \mathcal{M}$

$$\mathcal{T}_\rho \mathcal{M} := \left\{ \text{functions } \zeta \text{ on } \mathbb{R}^d \text{ satisfying } \int \zeta dx = 0 \right\}.$$

Since $\rho \geq 0$ is a probability density, the tangent space can also be identified as

$$\mathcal{T}_\rho \mathcal{M} := \left\{ \zeta = -\nabla \cdot (\rho \nabla u) + \rho \left(u - \int u \rho dx \right) \right\}.$$

Indeed, there is “one-to-one” correspondence between ζ and u , since for any ζ such that $\int \zeta dx = 0$, there exists $u \in H^1(d\rho)$ (determined uniquely up to a constant) solving

$$\zeta = -\nabla \cdot (\rho \nabla u) + \rho \left(u - \int u \rho dx \right).$$

Here $H^1(d\rho)$ denotes the space of functions u such that $\|u\|_{H^1(d\rho)}^2 := \int (|\nabla u|^2 + |u|^2) d\rho < \infty$. Informed by the Lagrangian minimization in the definition of the Wasserstein-Fisher-Rao distance (7), we also define the Riemannian metric tensor $g_\rho(\cdot, \cdot) : \mathcal{T}_\rho \mathcal{M} \times \mathcal{T}_\rho \mathcal{M} \rightarrow \mathbb{R}$ by

$$\begin{aligned} (A.1) \quad g_\rho(\zeta_1, \zeta_2) &:= \int_{\mathbb{R}^d} \rho \nabla u_1 \cdot \nabla u_2 dx + \int_{\mathbb{R}^d} \rho \left(u_1 - \int u_1 \rho dx \right) \left(u_2 - \int u_2 \rho dx \right) dx \\ &= \int_{\mathbb{R}^d} \rho \nabla u_1 \cdot \nabla u_2 dx + \int_{\mathbb{R}^d} u_1 u_2 \rho dx - \int_{\mathbb{R}^d} u_1 \rho dx \cdot \int_{\mathbb{R}^d} u_2 \rho dx, \end{aligned}$$

where $\zeta_i = -\nabla \cdot (\rho \nabla u_i) + \rho \left(u_i - \int u_i \rho dx \right)$, $i = 1, 2$. With this metric tensor g_ρ , the Wasserstein-Fisher-Rao distance defined by (7) can be regarded as the geodesic distance on \mathcal{M} with the Riemannian metric g_ρ , namely,

$$\begin{aligned} (A.2) \quad d_{\text{WFR}}^2(\rho_0, \rho_1) &= \left\{ \inf_{u_t} \int_0^1 g_{\rho_t}(\dot{\rho}_t, \dot{\rho}_t) dt \right. \\ &\quad \left. \text{s.t. } \dot{\rho}_t = -\nabla \cdot (\rho_t \nabla u_t) + \rho_t \left(u_t - \int_{\mathbb{R}^d} u_t \rho_t dx \right), \quad \rho_t|_{t=0} = \rho_0, \quad \rho_t|_{t=1} = \rho_1 \right\}. \end{aligned}$$

Proposition A.1. *Let $\mathcal{F} : \mathcal{M} \rightarrow \mathbb{R}$ be a continuous and differentiable energy functional. Then the metric gradient of $\mathcal{F}(\rho)$ via the metric tensor g_ρ is*

$$(A.3) \quad \text{grad}\mathcal{F}(\rho) = -\nabla \cdot \left(\rho \frac{\delta\mathcal{F}(\rho)}{\delta\rho} \right) + \rho \left(\frac{\delta\mathcal{F}(\rho)}{\delta\rho} - \int \frac{\delta\mathcal{F}(\rho)}{\delta\rho} \rho dx \right)$$

As a result, the gradient flow of $\mathcal{F}(\rho)$ with respect to the Wasserstein-Fisher-Rao distance d_{WFR} is given by

$$(A.4) \quad \begin{aligned} \partial_t \rho &= -\text{grad}\mathcal{F}(\rho) \\ &= \nabla \cdot \left(\rho \frac{\delta\mathcal{F}(\rho)}{\delta\rho} \right) - \rho \left(\frac{\delta\mathcal{F}(\rho)}{\delta\rho} - \int \frac{\delta\mathcal{F}(\rho)}{\delta\rho} \rho dx \right). \end{aligned}$$

Proof. Let $\rho_t : t \rightarrow \rho_t$ be a C^1 curve passing through $\rho_t|_{t=0} = \rho \in \mathcal{P}(\mathbb{R}^d)$ with tangent vector

$$\frac{d\rho_t}{dt}|_{t=0} = \zeta = -\nabla \cdot (\rho \nabla u) + \rho \left(u - \int u \rho dx \right).$$

The gradient $\text{grad}\mathcal{F}$ with respect to $g_\rho(\cdot, \cdot)$ is defined by

$$(A.5) \quad g_\rho(\text{grad}\mathcal{F}(\rho), \zeta) = \frac{d\mathcal{F}(\rho_t)}{dt}|_{t=0} = \int \frac{\delta\mathcal{F}(\rho)}{\delta\rho} \zeta dx.$$

By the definition of the Riemannian metric $g_\rho(\cdot, \cdot)$ in (A.1), the right hand side above is

$$\begin{aligned} \int \frac{\delta\mathcal{F}(\rho)}{\delta\rho} \zeta dx &= \int \frac{\delta\mathcal{F}(\rho)}{\delta\rho} \left[-\nabla \cdot (\rho \nabla \alpha) + \rho \left(\alpha - \int \alpha \rho dx \right) \right] dx \\ &= \int \rho \nabla \frac{\delta\mathcal{F}(\rho)}{\delta\rho} \cdot \nabla \alpha + \rho \left(\frac{\delta\mathcal{F}(\rho)}{\delta\rho} - \int \frac{\delta\mathcal{F}(\rho)}{\delta\rho} \rho dx \right) \alpha dx. \\ &= \int \rho \nabla \frac{\delta\mathcal{F}(\rho)}{\delta\rho} \cdot \nabla \alpha + \rho \left(\frac{\delta\mathcal{F}(\rho)}{\delta\rho} - \int \frac{\delta\mathcal{F}(\rho)}{\delta\rho} \rho dx \right) \left(\alpha - \int \alpha \rho dx \right) dx. \\ &= g_\rho \left(-\nabla \cdot \left(\rho \frac{\delta\mathcal{F}(\rho)}{\delta\rho} \right) + \left(\frac{\delta\mathcal{F}(\rho)}{\delta\rho} - \int \frac{\delta\mathcal{F}(\rho)}{\delta\rho} \rho dx \right), \zeta \right) \end{aligned}$$

Since ζ is arbitrary, this proves (A.3) and hence (A.4) follows. \square

Proof of Theorem 3.1. This is a direct consequence of Proposition A.1 and the fact that the functional derivative of $\rho \mapsto \text{KL}(\rho|\pi)$ is

$$\frac{\delta\text{KL}(\rho|\pi)}{\delta\rho} = \log \left(\frac{\rho}{\pi} \right) + 1.$$

\square

APPENDIX B. PROOFS OF CONVERGENCE RESULTS

In this section we prove Theorem 3.2, Theorem 3.3, Theorem 3.4, and Proposition 5.1.

Proof of Theorem 3.2. Differentiating $\text{KL}(\rho_t|\pi)$ in time gives

$$\frac{d}{dt} \text{KL}(\rho_t|\pi) = -\mathcal{I}(\rho_t|\pi) - \left(\int \rho_t \left| \log \frac{\rho_t}{\pi} \right|^2 dx \right) - \left(\int \rho_t \log \frac{\rho_t}{\pi} dx \right)^2.$$

Then the theorem is proved by using (4) and the fact the second term on the right side above is non-positive due to the Cauchy-Schwartz inequality. \square

Proof of Theorem 3.3. It suffices to assume $t_0 = 0$. First, we claim that if (10) holds, then for all $t > 0$:

$$(B.1) \quad \inf_{x \in \mathbb{R}^d} \frac{\rho_t(x)}{\pi(x)} \geq e^{-Me^{-t}}.$$

This is because the function $\eta_t(x) = \log(\rho_t(x)/\pi(x))$ satisfies

$$(B.2) \quad \partial_t \eta = \Delta \eta + b(t, x) \cdot \nabla \eta - \eta + \text{KL}(\rho_t|\pi) \geq \Delta \eta + b(t, x) \cdot \nabla \eta - \eta$$

where $b(t, x) = \nabla \log \rho_t(x)$. By the maximum principle, the minimum of η , which must be negative, cannot decrease. In fact, (10) and (B.2) implies $\eta_t(x) \geq e^{-t} \inf_x \eta_0(x) \geq -M e^{-t}$ so that $\rho_t(x)/\pi(x) \geq e^{-M e^{-t}}$, which is (B.1). In particular, if $t \geq t_1 = |\log(\delta/M)|$, then we have

$$(B.3) \quad \inf_{x \in \mathbb{R}^d} \rho_t(x)/\pi(x) \geq e^{-\delta}.$$

Now, under the evolution (6), the time derivative of $\text{KL}(\rho_t|\pi)$ is

$$(B.4) \quad \frac{d}{dt} \text{KL}(\rho_t|\pi) = \underbrace{-\mathcal{I}(\rho_t|\pi)}_{\leq 0} - \int \rho_t \left| \log \left(\frac{\rho_t}{\pi} \right) \right|^2 dx + \text{KL}(\rho_t|\pi)^2.$$

We may ignore the the first term on the right side since it is non-positive. Define $f_t = \frac{\rho_t}{\pi} - 1 \geq -1$. Then,

$$\text{KL}(\rho_t|\pi) = \int \rho_t \log \left(\frac{\rho_t}{\pi} \right) dx = \int ((1 + f_t) \log(1 + f_t) - f_t) \pi dx$$

and

$$\int \rho_t \left| \log \left(\frac{\rho_t}{\pi} \right) \right|^2 dx = \int (1 + f_t) |\log(1 + f_t)|^2 \pi dx.$$

Observe that the functions $H_1(f) = (1 + f) \log(1 + f) - f$ and $H_2(f) = (1 + f) |\log(1 + f)|^2$ are both non-negative for $f \geq -1$, $H_1'(0) = H_2'(0) = 0$, and $H_1''(f) = 1/(1 + f)$ and $H_2''(f) = 2(\log(1 + f) + 1)/(1 + f) \geq (2 - 2\delta)H_1''(f)$ if $f \geq e^{-\delta} - 1$. Therefore, we have

$$(2 - 2\delta)H_1(f) \leq H_2(f), \quad \text{if } f \geq e^{-\delta} - 1.$$

The condition (B.3) implies $\inf f_t(x) \geq e^{-\delta} - 1$ for all $t \geq t_1$. Combining these observations with (B.4), we see that

$$(B.5) \quad \begin{aligned} \frac{d}{dt} \text{KL}(\rho_t|\pi) &\leq - \int H_2(f_t) \pi dx + \text{KL}(\rho_t|\pi)^2 \\ &\leq - \int (2 - 2\delta)H_1(f_t) \pi dx + \text{KL}(\rho_t|\pi)^2 \\ &= -(2 - 2\delta)\text{KL}(\rho_t|\pi) + \text{KL}(\rho_t|\pi)^2 \end{aligned}$$

holds for all $t \geq t_1$. Since $\text{KL}(\rho_t|\pi) \leq \text{KL}(\rho_0|\pi) \leq 1$ also holds, by assumption, this implies

$$(B.6) \quad \frac{d}{dt} \text{KL}(\rho_t|\pi) \leq -(2 - 2\delta)\text{KL}(\rho_t|\pi) + \text{KL}(\rho_t|\pi) \leq -\frac{1}{2}\text{KL}(\rho_t|\pi)$$

for all $t \geq t_1$, so that $\text{KL}(\rho_t|\pi) \leq e^{-\frac{1}{2}(t-t_1)}\text{KL}(\rho_0|\pi) \leq e^{-\frac{1}{2}(t-t_1)}$. Now, returning to (B.5), we have

$$(B.7) \quad \frac{d}{dt} \text{KL}(\rho_t|\pi) \leq -(2 - 2\delta)\text{KL}(\rho_t|\pi) + e^{-\frac{1}{2}(t-t_1)}\text{KL}(\rho_t|\pi) \leq -(2 - 3\delta)\text{KL}(\rho_t|\pi)$$

for all $t \geq t_1 + 2|\log(\delta)| = \log(\frac{M}{\delta^3}) = t_*$. □

Proof of Theorem 3.4. If ρ_t satisfies (5), then

$$(B.8) \quad \frac{d}{dt} \text{KL}(\rho_t|\pi) = - \left(\int \rho_t \left| \log \frac{\rho_t}{\pi} dx \right|^2 - \left(\int \rho_t \log \frac{\rho_t}{\pi} dx \right)^2 \right) \leq 0.$$

So, $\text{KL}(\rho_t|\pi)$ is non-increasing and hence is finite since $\text{KL}(\rho_0|\pi)$ is finite. By the monotone convergence theorem there exists $C_* \geq 0$ such that $\lim_{t \rightarrow \infty} \text{KL}(\rho_t|\pi) = C_*$.

Next we show that the solution $\rho_t(x) > 0$ if $\rho_0(x) > 0$. Let us denote $\eta_t(x) = \log(\rho_t(x)/\pi(x))$. Then η_t solves the equation

$$(B.9) \quad \partial_t \eta_t = -\eta_t + \text{KL}(\rho_t|\pi).$$

Hence, η satisfies the relation

$$(B.10) \quad \eta_t(x) = e^{-t} \eta_0(x) + \int_0^t e^{-(t-s)} \text{KL}(\rho_s|\pi) ds, \quad \forall x \in \mathbb{R}^d, t > 0.$$

In particular, $t \mapsto \eta_t(x)$ is increasing if $\eta_t(x) < 0$, which implies that $\eta_t(x) \geq \min(0, \eta_0(x)) > -\infty$. As a result, $\rho_t(x) = e^{\eta_t(x)}\pi(x) > 0$, $\forall x \in \mathbb{R}^d$. In addition, since $0 \leq \text{KL}(\rho_t|\pi) \leq \text{KL}(\rho_0|\pi) < \infty$ and $\text{KL}(\rho_t|\pi) \rightarrow C_*$, we have

$$(B.11) \quad \lim_{t \rightarrow \infty} \int_0^t e^{-(t-s)} \text{KL}(\rho_s|\pi) ds = C_*.$$

Because of this and (B.10), we conclude that for any $x \in \mathbb{R}^d$, $\eta_t(x) \rightarrow C_*$ as $t \rightarrow \infty$, and $\rho_t(x) \rightarrow e^{C_*}\pi(x)$ as $t \rightarrow \infty$. However, since both π and ρ_t are probability densities, this implies $e^{C_*} = 1$, so that $C_* = 0$. Thus, $\lim_{t \rightarrow \infty} \rho_t(x) = \pi(x)$ and $\text{KL}(\rho_t|\pi) = C_* = 0$. \square

Proof of Proposition 5.1. We give a formal proof using the theory of measure-valued Markov process [13]; a similar proof strategy is used recently in [42]. Our goal is to first derive the (infinite dimensional) generator and the backward Kolmogorov equation of the measure-valued Markov process of $\mu_t^N = \frac{1}{N} \sum_{i=1}^N \delta_{x^i(t)}$. To this end, let us define for any smooth functional $\Psi : \mathcal{P}(\mathbb{R}^d) \rightarrow \mathbb{R}$ the generator \mathcal{L}_N

$$(\mathcal{L}_N \Psi)(\mu^N) := \lim_{t \downarrow 0} \frac{\mathbb{E}_0 \Psi(\mu_t^N) - \Psi(\mu^N)}{t},$$

where \mathbb{E}_0 denotes the expectation of $\Psi(\mu_t^N)$ conditioned on that $\mu_0^N = \mu^N$. To evaluate the limit above, notice that by definition whenever a particle x_t^i is killed (or duplicated) at time t , another particle x_t^j is duplicated (or killed) instantaneously. The birth or death is dictated by the sign of the birth-death rate $\Lambda(x^i)$ defined by (14). As a result, the instantaneous change from μ_{t-}^N to μ_t^N is

$$\mu_t^N - \mu_{t-}^N = -\frac{1}{N} \text{sign}(\Lambda(x^i)) (\delta_{x^i} - \delta_{x^j}).$$

It is thus useful to define the empirical measure after a swap happens between x and x' at time t by

$$(B.12) \quad \mu_t^N \{x \leftrightarrow x'\} = \mu_{t-}^N - \frac{1}{N} \text{sign}(\Lambda(x)) (\delta_x - \delta_{x'}).$$

Since the particles are undergoing Langevin diffusions independently before a swap occurs between x^i and x^j occurs with an exponential rate $\Lambda(x^i)$, we can derive that

$$(B.13) \quad \begin{aligned} (\mathcal{L}_N \Psi)(\mu^N) &= \frac{1}{N} \sum_{i=1}^N \int \left(\nabla_x D_{\mu^N} \Psi(x^i) \cdot \nabla \log \pi(x^i) + \Delta_x D_{\mu^N} \Psi(x^i) \right) \delta_{x^i}(dx) \\ &+ \frac{1}{N} \sum_{i,j=1}^N \iint |\Lambda(x^i)| \delta_{x^i}(dx) \delta_{x^j}(dx) \left(\Psi(\mu^N \{x^i \leftrightarrow x^j\}) - \Psi(\mu^N) \right), \end{aligned}$$

where the functional derivative $D_\mu \Psi(x)$ is a function from $\mathbb{R}^d \rightarrow \mathbb{R}$ defined by that for any signed measure ν with $\int \nu(dx) = 0$,

$$(B.14) \quad \lim_{\epsilon \rightarrow 0} \frac{\Psi(\mu + \epsilon \nu) - \Psi(\mu)}{\epsilon} = \int D_\mu \Psi(x) \nu(dx).$$

Now by the definition of the empirical measure μ^N , the generator \mathcal{L}_N can be rewritten as

$$(B.15) \quad \begin{aligned} (\mathcal{L}_N \Psi)(\mu^N) &= \int \left(\nabla_x D_{\mu^N} \Psi(x) \cdot \nabla \log \pi(x) + \Delta_x D_{\mu^N} \Psi(x) \right) \mu^N(dx) \\ &+ N \iint |\Lambda(x, \mu^N)| \mu^N(dx) \mu^N(dx') \left(\Psi(\mu^N \{x \leftrightarrow x'\}) - \Psi(\mu^N) \right), \end{aligned}$$

where $\Lambda(x, \mu)$ is defined by

$$\Lambda(x, \mu) = \log(K * \mu(x)) - \log \pi(x) - \int \left(\log(K * \mu(x)) - \log \pi(x) \right) \mu(dx).$$

Note that the measure $\mu^N\{x \leftrightarrow x'\}$ on the right side of (B.15) is defined in (B.12) with jump rate $\Lambda(x, \mu^N)$. With the generator, we can write the backward Kolmogorov equation on the observable $\Psi(\mu_t^N)$ as

$$\partial_t \Psi(\mu_t^N) = \mathcal{L}_N \Psi(\mu_t^N), \quad \Psi(\mu_t^N)|_{t=0} = \Psi(\mu_0^N).$$

Now passing to the limit $N \rightarrow \infty$ and assuming that $\mu_t^N \rightarrow \rho_t$ we claim that formally we have $(\mathcal{L}_N \Psi)(\mu_t^N) \rightarrow (\mathcal{L} \Psi)(\rho_t)$ where the limiting generator \mathcal{L} is given by

$$(B.16) \quad (\mathcal{L} \Psi)(\mu) = \int \left(\nabla_x D_\mu \Psi(x) \cdot \nabla \log \pi(x) + \Delta_x D_\mu \Psi(x) \right) \mu(dx) - \int \Lambda(x, \mu) \mu(dx) D_\mu \Psi(x).$$

In fact, by assumption the first term on the right side of (B.16) is the formal limit of the first term on the right side of (B.15). For the second term, one first sees from the definition of the functional derivative in (B.14) that as $N \rightarrow \infty$

$$\Psi(\mu^N\{x \leftrightarrow x'\}) - \Psi(\mu^N) \approx -\frac{1}{N} \int D_\mu \Psi(y) \text{sign}(\Lambda(x, \mu^N)) (\delta_x(dy) - \delta_{x'}(dy)).$$

This implies that as $N \rightarrow \infty$ the second term on the right side of (B.16) formally converges to

$$(B.17) \quad \begin{aligned} & - \iint |\Lambda(x, \mu)| \mu(dx) \mu(dx') \int D_\mu \Psi(y) \text{sign}(\Lambda(x, \mu)) (\delta_x(dy) - \delta_{x'}(dy)) \\ & = - \iint \int D_\mu \Psi(y) \Lambda(x, \mu) \delta_x(dy) \mu(dx) \mu(dx') + \iint \int D_\mu \Psi(y) \Lambda(x, \mu) \delta_{x'}(dy) \mu(dx) \mu(dx') \\ & = - \int D_\mu \Psi(x) \Lambda(x, \mu) \mu(dx), \end{aligned}$$

where the last line follows from the fact that

$$\iint \int D_\mu \Psi(y) \Lambda(x, \mu) \delta_{x'}(dy) \mu(dx) \mu(dx') = \int D_\mu \Psi(y) \mu(dy) \cdot \underbrace{\int \Lambda(x, \mu) \mu(dx)}_{=0} = 0$$

Combining above yields (B.16). Consequently, we obtain the mean field backward Kolmogorov equation

$$\partial_t \Psi(\rho_t) = (\mathcal{L} \Psi)(\rho_t), \quad \Psi(\rho_t)|_{t=0} = \Psi(\rho_0).$$

It is easy to check that this equation is precisely the time-evolution of $\Psi(\rho_t)$ where ρ_t solves (13). This shows that $\mu_t^N \rightarrow \rho_t$ and concludes the proof. \square

APPENDIX C. MORE DETAILS ON EXAMPLE 1

Let us first explain how we compute the numerical solutions of three continuous dynamics. The Fokker-Planck equation (3) is solved using the pseudo-spectral discretization in space and an implicit backward Euler discretization in time. The pure birth-death equation (5) is solved approximately by using the splitting scheme of alternating the following two steps:

Step 1: evolve the ODE system $\frac{d\rho_t(x)}{dt} = -\rho_t(\log \rho_t(x) - \log \pi(x))$ indexed by x for a small time step Δt .

Step 2: renormalize the solution by setting $\rho_t(x) \leftarrow \rho_t(x) / \int \rho_t(x) dx$.

When Δt is sufficiently small, this splitting scheme provides a good approximation to (5). The Fokker-Planck equation with birth-death (6) is solved by first evolving the Fokker-Planck equation (3) for a time step Δt using the pseudo-spectral method and then evolving the birth-death equation (5) using the splitting scheme above for another time step Δt . We use 500 spatial grids points in pseudo-spectral method and time step size 5×10^{-3} in time-marching.

We show in Figure C.5 some snapshots of solutions of three continuous dynamics and the corresponding particle algorithms for Example 1, which illustrates the acceleration effect of the birth-death dynamics on the Langevin dynamics.

We present another group of numerical results for Example 1 in Figure C.6 and Figure C.7, where we choose a Gaussian initial distribution with a larger variance $\sigma = 4$. As before, we find that our algorithm BDLS outperforms ULA. Observe that the particle algorithm BDS (based on pure birth-death dynamics) works also well in this case because the initial particles are spread out

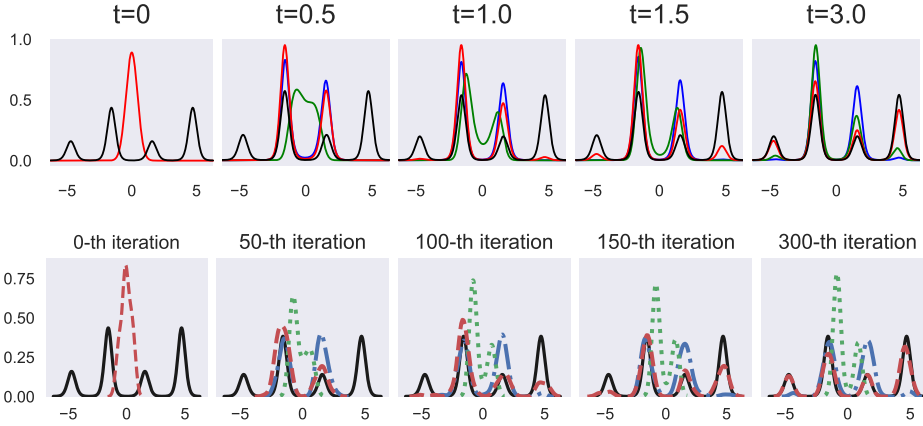


FIGURE C.5. Solutions of continuous dynamics (top row) at varying times and distributions (kernel density estimators) of the corresponding particle algorithms (bottom row) at different iterations in Example 1. The initial distribution is $\mathcal{N}(0, 0.2)$. The solid black lines are the target density and the blue (resp., blue dash-dot) lines are solutions of the FPE (resp., iterates of parallel ULA). The green and green dotted lines are solutions of BDE and the distributions of particles computed using BDS respectively. The red lines and red dashed lines are solutions of BDL-FPE and the distributions of particles computed using BDS respectively.

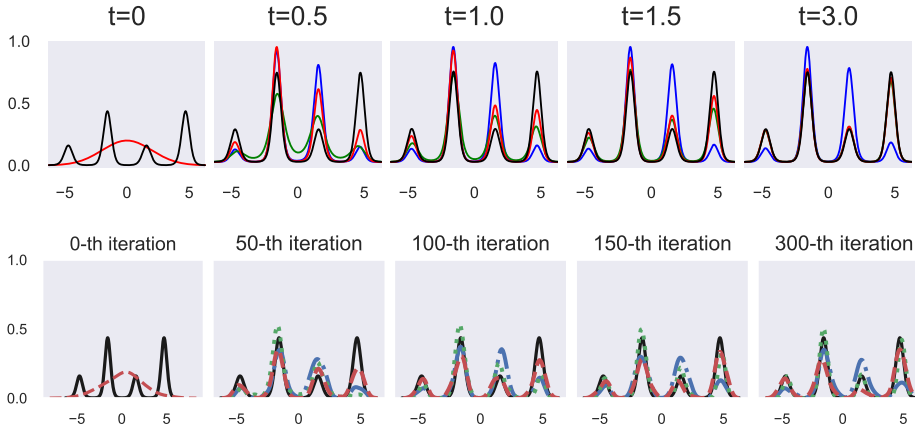


FIGURE C.6. The same setting as in Figure C.5 for Example 1 but with initial distribution $\mathcal{N}(0, 4)$. The solid black lines are the target density and the blue (resp., blue dash-dot) lines are solutions of the FPE (resp., iterates of parallel ULA). The green and green dotted lines are solutions of BDE and the particles generated using BDS respectively. The red lines and red dashed lines are solutions of BDL-FPE and particles generated using BDS respectively.

on the whole domain so that they can quickly cluster around different modes by rearranging their locations.

APPENDIX D. MORE DETAILS ON EXAMPLE 3

We provide more details on the Bayesian Gaussian mixture model used in Example 3. Let $y = \{y_1, \dots, y_n\}$ be a dataset consisting of an i.i.d. sequence of samples from the Gaussian

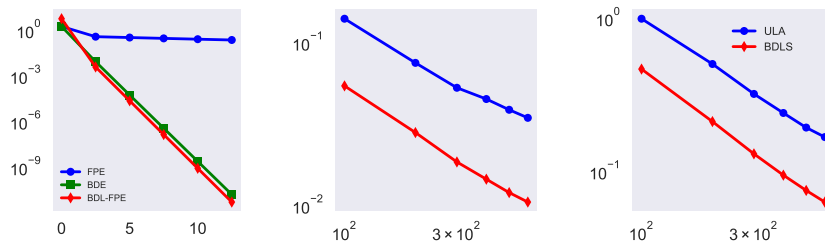


FIGURE C.7. The same setting as in Figure 1 for Example 1 but with initial distribution $\mathcal{N}(0, 4)$. The left figure shows decay of the KL divergence in semilogy scale along the evolution of three continuous dynamics. The middle (or the right) figure shows the decay in loglog scale of mean square errors of estimating mean (or variance) using varying number of particles.

mixture distribution

$$p(y|x) = \sum_{k=1}^3 w_k \mathcal{N}(y; \mu_k, \lambda_k^{-1})$$

where μ_k and $\lambda_k \geq 0$ are the means and precisions of the Gaussian components. The weights $\{w_k\}_{k=1}^3$ satisfy that $0 \leq w_k \leq 1$ and that $\sum_{k=1}^3 w_k = 1$. We denote by x the vector of parameters/hyperparameters in this model. We take the same prior distribution as in [11] and [25], namely for $k = 1, 2, 3$,

$$\mu_k \sim \mathcal{N}(m, \kappa^{-1}), \lambda_k \sim \text{Gamma}(\alpha, \beta), \beta \sim \text{Gamma}(g, h), (w_1, w_2) \sim \text{Dirichlet}_3(1, 1, 1).$$

We also choose $m = M, \kappa = 4/R^2, \alpha = 2, g = 0.02, h = 100g/(\alpha R^2)$, where R and M are the mean and range of the data y . By the Bayes' rule, the posterior is given by

$$(D.1) \quad p(x|y) \propto \beta^{3\alpha+g-1} \left(\prod_{k=1}^3 \lambda_k \right)^{\alpha-1} \exp \left(-\frac{\kappa}{2} \sum_{k=1}^3 (\mu_k - m)^2 - \beta \left(h + \sum_{k=1}^3 \lambda_k \right) \right) \\ \times \prod_{i=1}^n \left(\sum_{k=1}^3 w_k \lambda_k^{1/2} \exp \left(-\frac{\lambda_k}{2} (y_i - \mu_k)^2 \right) \right)$$

The unknown vector x of parameters is

$$x = (w_1, w_2, \mu_1, \mu_2, \mu_3, \lambda_1, \lambda_2, \lambda_3, \beta) \in \Omega := \mathcal{S}_3 \times \mathbb{R}^3 \times \mathbb{R}_+^4,$$

where $\mathbb{R}_+ = [0, \infty)$ and $\mathcal{S}_3 = \{(w_1, w_2) \in \mathbb{R}_+^2 \mid 0 \leq w_1 + w_2 \leq 1\}$ is the probability simplex in \mathbb{R}^2 . There are several issues in the implementation of ULA and BDLS. First, the constraints on w_k, λ_k and β may be violated if the vanilla ULA and BDLS are applied on the whole space without additional treatment during the evolution. Note also that the posterior density is not differentiable near the boundary of Ω . Moreover, even inside the domain Ω , the gradient of $\log \pi$ may not be globally Lipschitz, which may lead to non-ergodic Markov chains when applying ULA and BDLS. To overcome the latter issue, we use the following tamed ULA scheme [21]

$$x_{k+1} = x_k + \frac{\Delta t \nabla \log \pi(x_k)}{1 + \Delta t |\nabla \log \pi(x_k)|} + \sqrt{2\Delta t} \xi_k, k = 1, 2, \dots,$$

where $\xi_k \sim \mathcal{N}(0, 1)$. The small modification of the drift stabilizes the algorithm and makes the resulting Markov chain ergodic; see [21, 8] for more discussions about its convergence analysis.

To circumvent the constraint issue, we set a reflecting boundary at the origin for the parameters λ_k and β , i.e. we take the modulus of these parameters if they become negative. For the weight vector (w_1, w_2) , to improve sampling efficiency we slightly relax the strong constraint that $(w_1, w_2) \in \mathcal{S}_3$ and instead only require that $0 \leq w_k \leq 1, k = 1, 2$. We achieve this by setting

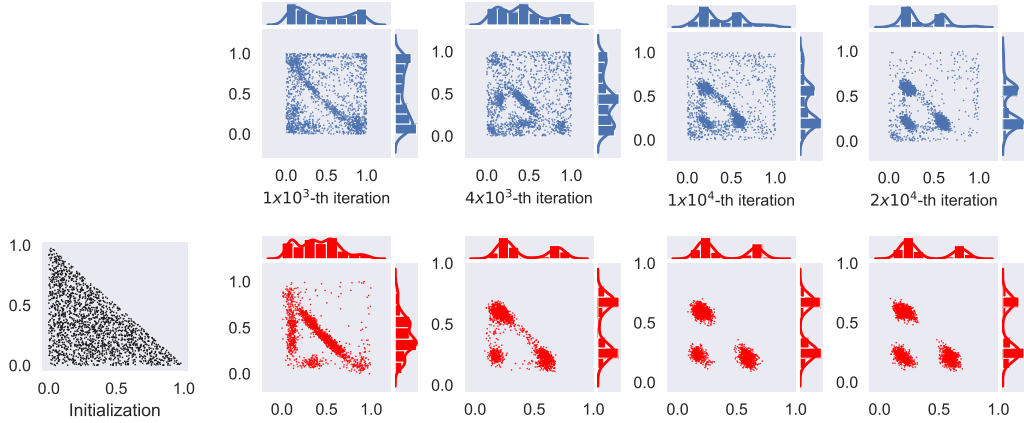


FIGURE D.8. Evolution of particles in (w_1, w_2) -coordinate for Example 3. The first column shows the initial particles in (w_1, w_2) -coordinate. The remaining columns compare the scatter plots of particles in (w_1, w_2) and their marginals computed using parallel ULA (blue) and BDLS (red) at different iterations. The constraint $0 \leq w_1 + w_2 \leq 1$ is relaxed to $0 \leq w_k \leq 1$ in implementing ULA and BDLS to boost sampling efficiency.

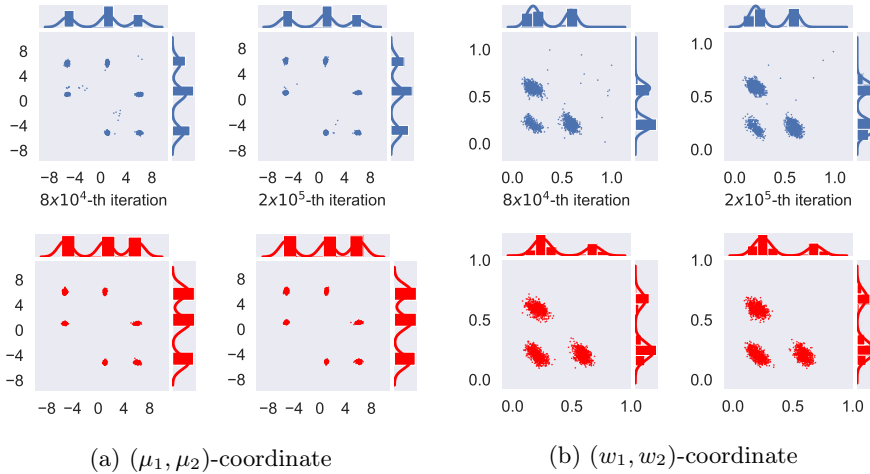


FIGURE D.9. Additional snapshots of particle evolution in (μ_1, μ_2) -coordinate and (w_1, w_2) -coordinate for Example 3. As in Figure 4, the top row (blue) and the bottom row (red) show the scatter plots of particles and their marginals computed using parallel ULA and BDLS respectively at larger iterations.

reflections on the boundary $w = 0$ and $w = 1$. Numerical experiments show that the relaxation does not break this constraint on the samplers near equilibrium; see Figure D.9b.

Finally we include several numerical results on Example 3 that are not fitted in the main paper. Figure D.8 compares the evolution of particles computed using parallel ULA and BDLS in (w_1, w_2) .

Figure D.9 displays the distribution of particles in (μ_1, μ_2) and in (w_1, w_2) at larger numbers of iterations (near equilibrium), which complements Figure 4 and Figure D.8 in illustrating the faster convergence of BDLS compared to ULA.

REFERENCES

- [1] H. C. Andersen. Molecular dynamics simulations at constant pressure and/or temperature. *The Journal of Chemical Physics*, 72(4):2384–2393, 1980.
- [2] M. Bauer, M. Bruveris, and P. W. Michor. Uniqueness of the Fisher-Rao metric on the space of smooth densities. *Bull. Lond. Math. Soc.*, 48(3):499–506, 2016.
- [3] J. Bierkens, P. Fearnhead, and G. Roberts. The Zig-Zag process and super-efficient sampling for Bayesian analysis of big data. *Ann. Statist.*, 47:1288–1320, 2019.
- [4] A. Bouchard-Cote, S. J. Vollmer, and A. Doucet. The bouncy particle sampler: a nonreversible rejection-free Markov chain Monte Carlo method. *J. Amer. Statist. Assoc.*, 113:855–867, 2018.
- [5] A. Bovier, M. Eckhoff, V. Gayrard, and M. Klein. Metastability in reversible diffusion processes. I. Sharp asymptotics for capacities and exit times. *J. Eur. Math. Soc. (JEMS)*, 6(4):399–424, 2004.
- [6] A. Bovier, V. Gayrard, and M. Klein. Metastability in reversible diffusion processes. II. Precise asymptotics for small eigenvalues. *J. Eur. Math. Soc. (JEMS)*, 7(1):69–99, 2005.
- [7] Y. Brenier and D. Vorotnikov. On optimal transport of matrix-valued measures. *arXiv preprint arXiv:1808.05064*, 2018.
- [8] N. Brosse, A. Durmus, Éric Moulines, and S. Sabanis. The tamed unadjusted langevin algorithm. *Stochastic Processes and their Applications*, 2018.
- [9] X. Cheng, N. S. Chatterji, P. L. Bartlett, and M. I. Jordan. Underdamped Langevin MCMC: A non-asymptotic analysis. In S. Bubeck, V. Perchet, and P. Rigollet, editors, *Proceedings of the 31st Conference On Learning Theory*, volume 75 of *Proceedings of Machine Learning Research*, pages 300–323. PMLR, 06–09 Jul 2018.
- [10] L. Chizat, G. Peyré, B. Schmitzer, and F.-X. Vialard. An interpolating distance between optimal transport and Fisher-Rao metrics. *Found. Comput. Math.*, 18(1):1–44, 2018.
- [11] N. Chopin, T. Lelièvre, and G. Stoltz. Free energy methods for bayesian inference: efficient exploration of univariate gaussian mixture posteriors. *Statistics and Computing*, 22(4):897–916, Jul 2012.
- [12] A. S. Dalalyan. Theoretical guarantees for approximate sampling from smooth and log-concave densities. *Journal of the Royal Statistical Society: Series B (Statistical Methodology)*, 79(3):651–676, 2017.
- [13] D. A. Dawson. Measure-valued Markov processes. In *École d’Été de Probabilités de Saint-Flour XXI—1991*, volume 1541 of *Lecture Notes in Math.*, pages 1–260. Springer, Berlin, 1993.
- [14] P. Del Moral, A. Doucet, and A. Jasra. Sequential Monte Carlo samplers. *J. R. Statist. Soc. B*, 68:411–436, 2006.
- [15] A. Durmus and E. Moulines. Nonasymptotic convergence analysis for the unadjusted Langevin algorithm. *The Annals of Applied Probability*, 27(3):1551–1587, 2017.
- [16] R. Dwivedi, Y. Chen, M. J. Wainwright, and B. Yu. Log-concave sampling: Metropolis-Hastings algorithms are fast! In S. Bubeck, V. Perchet, and P. Rigollet, editors, *Proceedings of the 31st Conference On Learning Theory*, volume 75 of *Proceedings of Machine Learning Research*, pages 793–797. PMLR, 06–09 Jul 2018.
- [17] M. I. Freidlin and A. D. Wentzell. *Random perturbations of dynamical systems*, volume 260 of *Grundlehren der Mathematischen Wissenschaften [Fundamental Principles of Mathematical Sciences]*. Springer-Verlag, New York, 1984. Translated from the Russian by Joseph Szücs.
- [18] T. O. Gallouët and L. Monsaingeon. A JKO splitting scheme for Kantorovich-Fisher-Rao gradient flows. *SIAM J. Math. Anal.*, 49(2):1100–1130, 2017.
- [19] C. J. Geyer. Markov chain Monte Carlo maximum likelihood. In E. M. Keramidas, editor, *Computing Science and Statistics: Proc. 23rd Symposium on the Interface*, pages 156–163. Interface Foundation, Fairfax Station, VA, 1991.
- [20] G. S. Grest and K. Kremer. Molecular dynamics simulation for polymers in the presence of a heat bath. *Phys. Rev. A*, 33:3628–3631, 1986.
- [21] M. Hutzenthaler, A. Jentzen, and P. E. Kloeden. Strong convergence of an explicit numerical method for sdes with nonglobally lipschitz continuous coefficients. *Ann. Appl. Probab.*, 22(4):1611–1641, 08 2012.
- [22] R. Jordan, D. Kinderlehrer, and F. Otto. The Variational Formulation of the Fokker–Planck Equation. *SIAM Journal on Mathematical Analysis*, 29(1):1–17, 1998.
- [23] S. Kondratyev, L. Monsaingeon, and D. Vorotnikov. A fitness-driven cross-diffusion system from population dynamics as a gradient flow. *J. Differential Equations*, 261(5):2784–2808, 2016.
- [24] A. Laio and M. Parrinello. Escaping free-energy minima. *Proceedings of the National Academy of Sciences*, 99(20):12562–12566, 2002.
- [25] B. Leimkuhler, C. Matthews, and J. Weare. Ensemble preconditioning for Markov chain Monte Carlo simulation. *Stat. Comput.*, 28(2):277–290, 2018.
- [26] M. Liero, A. Mielke, and G. Savaré. Optimal transport in competition with reaction: the Hellinger-Kantorovich distance and geodesic curves. *SIAM J. Math. Anal.*, 48(4):2869–2911, 2016.
- [27] Q. Liu. Stein variational gradient descent as gradient flow. *Advances in Neural Information Processing Systems (NIPS 2017)*, 30, 2017.
- [28] Q. Liu and D. Wang. Stein variational gradient descent: A general purpose bayesian inference algorithm. *Advances in Neural Information Processing Systems (NIPS 2016)*, 29, 2016.
- [29] J. Lu, Y. Lu, and J. Nolen. Scaling limit of the Stein variational gradient descent: the mean field regime. *SIAM J. Math. Anal.*, 51:648–671, 2019.

- [30] Y.-A. Ma, T. Chen, and E. Fox. A complete recipe for stochastic gradient MCMC. In C. Cortes, N. D. Lawrence, D. D. Lee, M. Sugiyama, and R. Garnett, editors, *Advances in Neural Information Processing Systems 28*, pages 2917–2925. Curran Associates, Inc., 2015.
- [31] O. Mangoubi and A. Smith. Rapid mixing of Hamiltonian Monte Carlo on strongly log-concave distributions, 2017. preprint, arXiv:1708.07114.
- [32] E. Marinari and G. Parisi. Simulated tempering: a new Monte Carlo scheme. *Eur. Lett.*, 19:451–458, 1992.
- [33] G. S. Matthias Liero, Alexander Mielke. Optimal entropy-transport problems and a new hellinger–kantorovich distance between positive measures. *Invent. Math.*, 211(3):969–1117, 2018.
- [34] G. Menz and A. Schlichting. Poincaré and logarithmic Sobolev inequalities by decomposition of the energy landscape. *Ann. Probab.*, 42(5):1809–1884, 2014.
- [35] R. M. Neal. Annealed importance sampling. *Statistics and Computing*, 11(2):125–139, Apr. 2001.
- [36] R. M. Neal. *MCMC using Hamiltonian dynamics*, chapter 5. Chapman and Hall/CRC, 2011.
- [37] J. P. Nilmeier, G. E. Crooks, D. D. L. Minh, and J. D. Chodera. Nonequilibrium candidate Monte Carlo is an efficient tool for equilibrium simulation. *Proceedings of the National Academy of Sciences*, 108(45):E1009–E1018, 2011.
- [38] J. R. Norris. Long-time behaviour of heat flow: global estimates and exact asymptotics. *Arch. Rational Mech. Anal.*, 140(2):161–195, 1997.
- [39] F. Otto. The geometry of dissipative evolution equations: The porous medium equation. *Communications in Partial Differential Equations*, 26(1-2):101–174, 2001.
- [40] G. O. Roberts and R. L. Tweedie. Exponential convergence of Langevin distributions and their discrete approximations. *Bernoulli*, 2(4):341–363, 1996.
- [41] P. J. Rossy, J. D. Doll, and H. L. Friedman. Brownian dynamics as smart Monte Carlo simulation. *J. Chem. Phys.*, 69:4628, 1978.
- [42] G. Rotskoff, S. Jelassi, J. Bruna, and E. Vanden-Eijnden. Global convergence of neuron birth-death dynamics, 2019. preprint, arXiv:1902.01843.
- [43] R. H. Swendsen and J.-S. Wang. Replica Monte Carlo simulation of spin-glasses. *Phys. Rev. Lett.*, 57:2607–2610, 1986.
- [44] F. Wang and D. P. Landau. Efficient, multiple-range random walk algorithm to calculate the density of states. *Phys. Rev. Lett.*, 86:2050, 2001.
- [45] M. Welling and Y. W. Teh. Bayesian learning via stochastic gradient langevin dynamics. In *Proceedings of the 28th International Conference on International Conference on Machine Learning, ICML’11*, pages 681–688, USA, 2011. Omnipress.

(Y. Lu) DEPARTMENT OF MATHEMATICS, DUKE UNIVERSITY, DURHAM NC 27708, USA
E-mail address: yulonglu@math.duke.edu

(J. Lu) DEPARTMENT OF MATHEMATICS, DEPARTMENT OF PHYSICS AND DEPARTMENT OF CHEMISTRY, DUKE UNIVERSITY, DURHAM NC 27708, USA
E-mail address: jianfeng@math.duke.edu

(J. Nolen) DEPARTMENT OF MATHEMATICS, DUKE UNIVERSITY, DURHAM NC 27708, USA
E-mail address: nolen@math.duke.edu